DNA supercoiling enhances cooperativity and efficiency of an epigenetic switch

Kamilla Norregaard[a], Magnus Andersson[a,b], Kim Sneppen[a], Peter Eigil Nielsen[c], Stanley Brown[d], and Lene B. Oddershede[a,1]

[a]The Niels Bohr Institute, University of Copenhagen, 2100 Copenhagen, Denmark; [b]Department of Physics, Umeå University, SE-901 87 Umeå, Sweden; and [c]Department of Cellular and Molecular Medicine, Faculty of Health and Sciences and [d]Department of Biology, University of Copenhagen, 2200 Copenhagen, Denmark

Edited by Sankar Adhya, National Institutes of Health, National Cancer Institute, Bethesda, MD, and approved July 8, 2013 (received for review September 12, 2012)

Bacteriophage λ stably maintains its dormant prophage state but efficiently enters lytic development in response to DNA damage. The mediator of these processes is the λ repressor protein, CI, and its interactions with λ operator DNA. This λ switch is a model on the basis of which epigenetic switch regulation is understood. Using single molecule analysis, we directly examined the stability of the CI-operator structure in its natural, supercoiled state. We marked positions adjacent to the λ operators with peptide nucleic acids and monitored their movement by tethered particle tracking. Compared with relaxed DNA, the presence of supercoils greatly enhances juxtaposition probability. Also, the efficiency and cooperativity of the λ switch is significantly increased in the supercoiled system compared with a linear assay, increasing the Hill coefficient.

epigentic switch | autoregulation | repression | kinetics | gene regulation

Developmental programs are decision-making processes, primarily controlled by epigenetic switches. Once a cell differentiates, its daughter cells continue the developmental program. The decision between the dormant state (the lysogenic state) and the vegetative state (the lytic state) made by bacteriophage λ upon infection of an *Escherichia coli* was the first epigenetic switch to be deciphered (1) and continues to provide insights into biological processes (2, 3). Once the lysogenic state is established, it is exceptionally stable and departure in the absence of the DNA damage sensing system is nearly always caused by mutation (4–6). Maintenance of lysogeny is mediated by the λ repressor protein, CI, and its formation of a complex with phage DNA. The CI protein binds at two regulatory regions called operator right (OR) and operator left (OL), located about 2.3 kbp apart on the phage genome. Each operator is a constellation of three adjacent subsites that each bind dimers of CI in a hierarchical manner (1, 7). In a lysogenic cell, CI prevents lytic growth by directly repressing the lytic promoters pR and pL. This repression is enhanced by long-range cooperative interactions between CI dimers bound to the OL1–OL2 and OR1–OR2 regions, thus looping the DNA that lies between them (8) (Fig. 1 *A* and *B*). CI-mediated DNA looping brings OR3 in proximity to OL3. This juxtaposition allows a CI dimer bound to the strong OL3 to facilitate another CI dimer to bind to the intrinsically weak OR3, thus reducing the concentration of CI necessary to occupy OR3. In this manner CI can autoregulate its own expression by binding to OR2 (activation) or by binding to OR3 (repression). This autoregulation is crucial for the phage to maintain repression while preventing excessive accumulation of CI. When DNA in the lysogen is damaged, the bacterial DNA-damage–sensing system is triggered, leading to CI inactivation by self-cleavage (9) and to an efficient switch to the lytic state, eventually leading to production of progeny phage and cell death (1).

The switch from the lysogenic to the lytic state must be decisive. Partial entry into vegetative growth may kill the host without producing a full burst of progeny phage. Because the in vivo state of DNA is supercoiled (10), we sought to examine protein-mediated DNA looping on native, supercoiled DNA. In vitro single molecule experiments addressing looping have revealed important information regarding looping dynamics (11–14). However, previous experiments all used linear nonsupercoiled DNA or linear DNA where supercoils were mechanically introduced—for example, by twisting a bead attached to the end of a DNA tether (15–17). We developed a unique peptide nucleic acid (PNA)-based assay by which the long-range CI-mediated DNA looping can be measured directly in vitro on a naturally supercoiled DNA plasmid (sketched in Fig. 1*C*). For each plasmid molecule the degree of supercoiling is constant, hence, the change in overall length between the operator sites is due to CI-mediated looping only and not due to the introduction of additional supercoils.

After CI binding to the operators, loop formation can be divided into two steps: juxtaposition of the λ operators and closing the loop by protein interactions. As protein–protein binding is a fast process, site juxtaposition is believed to be the rate-limiting step (18). Supercoiled DNA is a compacted state; thus, many pairs of sites, although separated along the DNA contour, are positioned in close vicinity to each other. In comparison, a relaxed DNA of the same size is less compact and bears a much smaller number of juxtaposed sites. Brownian dynamics simulations scrutinizing the thermal motion of relaxed and supercoiled DNA suggest a dynamic difference between the two (19). The simulations predicted that site juxtaposition is in general a slow process, which is accelerated by supercoiling. Thus, supercoiling is expected to enhance loop formation. Using our naturally supercoiled plasmid system, we found the juxtaposition probability is greatly enhanced in a supercoiled plasmid in comparison with a

Significance

Bacteriophage λ was the first epigenetic switch to be deciphered and continues to contribute to our understanding of gene regulation. Its dormant state is exceptionally stable. In spite of this stability, viral development is efficiently activated in response to DNA damage. This ability to respond efficiently is due to a long-range protein-mediated DNA looping. We developed a single molecule assay based on peptide nucleic acid tethering of a naturally supercoiled DNA plasmid. The internal kinetics of the supercoiled plasmid was monitored, and the dynamics and stability of regulatory protein-mediated DNA looping investigated. We found that the DNA loop becomes tolerant to reductions in the regulator when DNA is supercoiled, thus helping explain the bistable nature of the lambda switch.

Author contributions: P.E.N., S.B., and L.B.O. designed research; K.N., M.A., and S.B. performed research; K.S., P.E.N., and S.B. contributed new reagents/analytic tools; K.N., M.A., and L.B.O. analyzed data; and K.N., M.A., S.B., and L.B.O. wrote the paper.

The authors declare no conflict of interest.

This article is a PNAS Direct Submission.

[1]To whom correspondence should be addressed. E-mail: oddershede@nbi.dk.

This article contains supporting information online at www.pnas.org/lookup/suppl/doi:10.1073/pnas.1215907110/-/DCSupplemental.

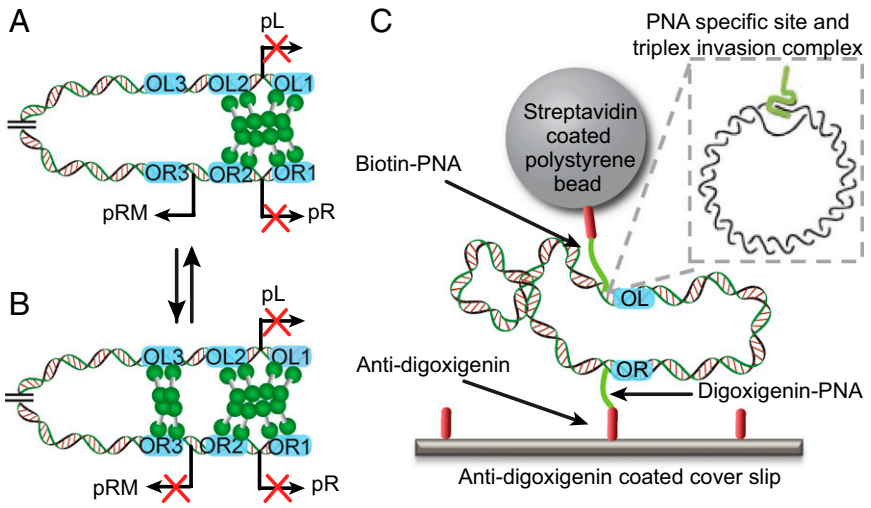

Fig. 1. A schematic of CI autoregulation by DNA looping and the experimental assay. Protein complex formation between the λ operator sites displaces the intervening DNA in a loop. The in vivo distance between the operators is ~2.3 kbp. The bent arrows show the transcription start points of the lytic promoters pL and pR and the lysogenic promoter pRM. The blue rectangles show the adjacent operator subsites OL1, OL2, OL3 and OR1, OR2, OR3. Red X signifies that the promoter is turned off in the shown configuration. CI dimers are shown as green dumbbell structures. (*A*) Octamer-mediated DNA looping by CI tetramers binding to OL1–OL2 and OR1–OR2. The lytic promoters, pL and pR, are repressed while CI transcription is activated by CI bound to OR2. (*B*) After octamer-mediated loop formation, an additional CI tetramer can bind cooperatively between OL3 and OR3, thus forming the octamer+tetramer complex. This represses both lytic genes and CI synthesis. (*C*) A plasmid DNA is tethered to an antidigoxigenin-coated cover slide via a digoxigenin–PNA and a streptavidin-coated μm-sized polystyrene bead via a biotin–PNA. The plasmids contain the entire λ immunity region and the two λ operators, OL and OR, flanked by the PNA-specific sites. CI dimers binding at OL and OR introduce loop formation and cause a detected decrease in the distance between the bead and the surface. (*C*, *Inset*) The PNA binds with sequence specificity to a DNA target and forms a triplex invasion complex while displacing the noncomplementary DNA strand in a loop.

relaxed plasmid. A supercoiled plasmid DNA has fewer accessible states and all available states are more rapidly explored than for a relaxed plasmid DNA.

Furthermore, we found that the presence of supercoils on DNA greatly enhances the looping probability at all investigated CI concentrations until saturation, in comparison with the looping probability of linear DNA (14). In particular at low concentrations (~20–40 nM) of CI monomers, the probability of being in the looped state is significantly higher for the supercoiled DNA, and the concentration interval where both the looped and unlooped states occur with significant probability is decreased. Hence, supercoiling facilitates looping at low CI concentrations and causes the switch between the looped and unlooped states to be sharper. Our findings are in accordance with an existing thermodynamic model (14, 20, 21), and we identified thermodynamic parameters that needed revision to make the model more compatible with in vivo observations (21, 22). The Hill coefficient characterizing the supercoiled assay ($h = 2.5$) is significantly higher than for the linear assay ($h = 1.2$), thus rendering the transition between states in a supercoiled system more robust to biological noise.

Results

PNA-Plasmid Assay. To examine binding of CI protein to DNA in its native, supercoiled state, we used two "handles" to monitor the dynamics of DNA at designated positions. The handles were made of bis-PNA, one bearing a biotin and the other a digoxigenin at its N terminus (Fig. 1*C*). Triplex invasion complexes formed between the homopyrimidine bis-PNA and DNA and resulted in an internal PNA–DNA–PNA triplex in which two PNA strands hybridized to the complementary DNA strand by combined Watson Crick and Hoogsteen base pairing (23) (Fig. 1*C*, *Inset*). Consequently, the noncomplementary DNA strand was displaced as a small, single stranded loop (24). A plasmid was constructed that contained the λ immunity region including the λ operators, OL and OR. On each side of the immunity region, unique PNA binding sites were engineered. Via a biotin-conjugated PNA, the plasmid was attached to a streptavidin-coated bead and via a digoxigenin-conjugated PNA to an antidigoxigenin-coated surface. The bound plasmid was torsionally constrained because the streptavidin bead was too large to rotate through the DNA plasmid circle.

A series of experiments was performed to determine the specificity and stability of the triplex invasion complexes. First, electrophoretic mobility shift experiments were conducted to identify initial solution conditions for accurate and efficient binding of both PNAs to their target sites (*SI Text* and Fig. S1). Next, two plasmids were prepared, one lacking the digoxigenin–PNA target (pSB4293) and another lacking the biotin–PNA target (pSB4300). Tethers were only expected to form with the plasmid bearing both PNA targets, pSB4312, and we used particle tracking to follow the motion of individual beads possibly tethered by each of the three plasmids. The excursions of the bead were analyzed by a principal component analysis as detailed in ref. 25 and in *SI Text*. Fig. S2 shows the 2D projected positions visited by the tethered bead, a typical time series, and a position histogram. The analysis yielded a number for the root mean square deviation (RMSD) of the bead from the center of its excursions, presumably the anchoring point. The larger the RMSD, the longer the overall length of the DNA tether. The RMSDs for each of the control plasmids as well as for pSB4312 are shown in Fig. S3. We found that the RMSD distribution from a sample with pSB4312 containing both PNA targets showed a bimodal distribution, the two peaks being separated by a large value. We attributed the peak representing the long excursions (RMSD > 150 nm) as stemming from correctly formed DNA–PNA tethers. The other peak representing short or no excursions of the bead (RMSD < 100 nm) was interpreted as originating from nonspecifically tethered beads. The presence of this lower peak is consistent with the RMSD distribution obtained from a control sample containing only beads and no DNA. The two control plasmids each lacking one PNA target only had the lower peak corresponding to unspecific bead attachments. The percentage of tethers with an RMSD above 150 nm out of the total number of tethers was 48% for pSB4312, whereas it was 4% and 8% for pSB4300 and pSB4293, respectively. A Student *t* test showed that the likelihood that the distribution observed with plasmids bearing both PNA targets is the same as the distribution observed with plasmids bearing only one of the PNA targets is $<6\times10^{-8}$. Hence, correct PNA targets were a prerequisite for formation of DNA tethers and the PNAs were binding to their designated target sites.

Juxtaposition Kinetics of Relaxed and Supercoiled DNA. First, we investigated the dynamics of supercoiled plasmids versus that of relaxed plasmids. For this purpose we prepared a smaller plasmid (pSB4357) containing 5,546 base pairs; 2.6 kbp containing the λ

immunity region was on one of the arcs connecting the bead and the surface and 2.9 kbp was on the other arc. Two types of experiments were carried out, one with the plasmid in its native supercoiled state and the other using a plasmid that was relaxed by nicking with the single strand endonuclease Nt.BspQI (pSB4357-R). PNA–DNA binding has a 2 order of magnitude higher binding rate to negatively supercoiled DNA compared with relaxed DNA (26). This is because PNA binding to DNA requires opening of the DNA helix and therefore PNA strand invasion is more efficient (faster) in the negatively supercoiled state in which strand separation is facilitated. For this reason higher PNA concentrations are needed for binding PNA handles to the relaxed tether. Also, by PCR we constructed a linear control DNA molecule with the same length (2.6 kbp) as the short of the arcs on pSB4357. All DNA constructs were examined in tethering experiments.

Inspired by the literature (25, 27) and the results from Fig. S3, we imposed the following selection criteria to minimize the occurrence of unspecific tethers in the analyzed datasets: (*i*) Results from beads that probably were attached directly to the surface, or by unspecific tethers, and hence had a small RMSD were discarded, and (*ii*) if the positions visited by the bead displayed a low degree of symmetry (s) as defined in *SI Text*, the bead might be attached to the surface by more than one DNA tether and the time series was discarded. More specifically, we set the RMSD threshold to RMSD > 60 nm and symmetry threshold to $s > 0.8$.

The RMSD of 83 beads tethered to the supercoiled plasmid pSB4357 and of 31 beads tethered by the relaxed plasmid pSB4357-R are plotted in the histograms shown in Fig. 2 *A* and *B*. The two RMSD histograms have mean values of 242 ± 46 nm (mean ± SD) for the supercoiled plasmid and 276 ± 39 nm for the relaxed plasmid, respectively. A Student t test on the two distributions returned a P value of 2.1×10^{-4}; therefore, the two distributions are significantly different. The RMSD of the relaxed pSB4357-R plasmid was compared with the RMSD of the linear control DNA molecule, 315 ± 26 nm. As the length of the linear control DNA molecule is identical to that of the short arc of pSB4357, it is reasonable that the means of the two RMSDs within the error bars are identical. Due to the semistiff nature of the DNA and the fact that the length of the arc is only around 17 DNA persistence lengths, it is, however, also reasonable that the excursions of the relaxed plasmid on average are a little smaller than those of the linear tether.

The broad distribution of RMSD observed for supercoiled DNA may be due to the broad distribution of supercoiled states in our plasmids as extracted from the bacteria. Due to the geometrical constraints on the system, once extracted, the degree of supercoiling (the writhe number) of each plasmid remained constant. Of all the plasmids, 99% contained at least one supercoil. To quantify the in vivo spread in writhe, we performed a chloroquine gel analysis, and the result is shown in Fig. 2*C* (the entire gel is shown in Fig. S4). For a particular plasmid preparation, the appearance of at least 10 distinct bands indicated that at least 10 different writhe numbers were present. The broad distribution of supercoiled states also gave rise to a broad distribution of tether lengths in the presence of CI protein.

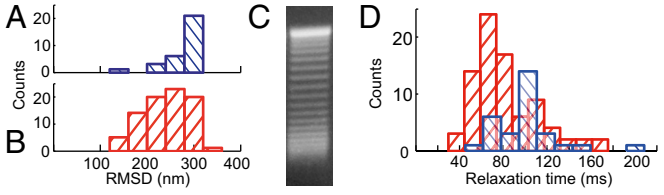

Fig. 2. Juxtaposition kinetics of supercoiled versus relaxed DNA. Histograms of the RMSD for the relaxed plasmid pSB4357-R (*A*) and for the naturally supercoiled plasmid pSB4357 (*B*). (*C*) Portion of chloroquine gel showing distribution of supercoils in the pSB4357 preparation. Entire electrophoretic gel shown is in Fig. S4. (*D*) Histogram of the relaxation time for all used datasets of pSB4357 (supercoiled plasmid; red) and pSB4357-R (relaxed plasmid; blue).

To investigate the intrinsic dynamics of supercoiled plasmids compared with that of relaxed plasmids, the autocorrelation between the positions in the time series was calculated: $C(\tau) \propto x(t+\tau)x(t) \propto \exp\left(\frac{-t}{\tau}\right)$. The relaxation time, τ, describes how long a system retains prior information and was extracted from fitting the latter expression to the time series. The autocorrelation of supercoiled DNA falls off faster than for relaxed DNA (Fig. S5). The calculated relaxation times were plotted in histograms (Fig. 2*D*) and the mean values (±1 SD) of τ for supercoiled and relaxed plasmids were found to be 81 ± 30 ms and 100 ± 30 ms, respectively. A Student t test comparing relaxation times between pSB4357 and pSB4357-R returned a P value $<3.1\times10^{-3}$, thus showing that the correlation times characterizing the two plasmids were significantly different. The supercoiled plasmid has a shorter relaxation time than the relaxed plasmid, representing faster internal motion of the supercoiled plasmid and thus a more rapid exploration of all available states. The relaxation time of the linear DNA molecule corresponding to the shorter arc of pSB4357 was 129 ± 49 ms. This value is significantly larger than that of the relaxed plasmid ($P = 8.0\times10^{-3}$) and reflects the influence of the geometrical constraints on the plasmid compared with the linear tether. These findings support the idea, consistent with previously proposed models (19), that juxtaposition kinetics are dependent on supercoiling as the internal motion of a DNA molecule is accelerated when the DNA is supercoiled. This is important as the frequency of site juxtaposition, in this case operator site juxtaposition, is believed to be a key factor in the occurrence of DNA looping (16, 18, 28).

CI-Mediated DNA Looping of Supercoiled Plasmids. In our assay, DNA looping mediated by CI proteins could be directly measured by a decrease in the overall length of the plasmid tether. To quantify protein clamping, we used a time-dependent measure, $\rho(t)$, to quantify the 2D projected length of the plasmid tether at time t. Whereas RMSD gives an average tether length during the entire time series, $\rho(t)$ measures the plasmid extension at time t. More precisely, we defined $\rho^2(t) = (x(t) - \langle x \rangle)^2 + (y(t) - \langle y \rangle)^2$, where the averages $\langle x \rangle$ and $\langle y \rangle$ were taken over the entire time series and hence designate the anchor point. To obtain the average value of ρ in a narrow window around t, $\rho(t)$ was filtered by a sliding window of 20 ms. The 2D projected physical distance between the tethering point and the position of the bead around time t is denoted $\sqrt{\langle \rho^2(t) \rangle_{20ms}}$ and is the quantity plotted in Fig. 3. As in the RMSD analysis we invoked a criterion on the projected length set to $\rho > 60$ nm. We often observed a decrease in the symmetry upon the CI clamping. Therefore, the criterion for s previously stated ($s > 0.8$) was used to select tethers before adding CI; however, after adding CI, the symmetry criterion was relaxed to $s > 0.6$.

To compare our data to single molecule studies on linear DNA tethers (14), we varied the CI concentrations from 5 to 170 nM (close to the estimated physiological concentration of CI monomers in a lysogenic cell, which is ~ 200 nM) (29, 30). The same bead tethered by pSB4357 was monitored up to 20 min after CI protein was added.

Typical $\sqrt{\langle \rho^2(t) \rangle_{20ms}}$ time series for different CI concentrations and their corresponding histograms are shown in Fig. 3 *A* and *B*. The histogram of the control experiments without CI is shown in Fig. 2*B* and additional time series for all tested concentrations of CI are shown in Fig. S6. All tethers had maximum excursions smaller than the 2.6 kbp linear DNA molecule; however, as the individual tethers displayed a relatively large distribution of degree of supercoiling (as shown in Fig. 2*C*), the overall length

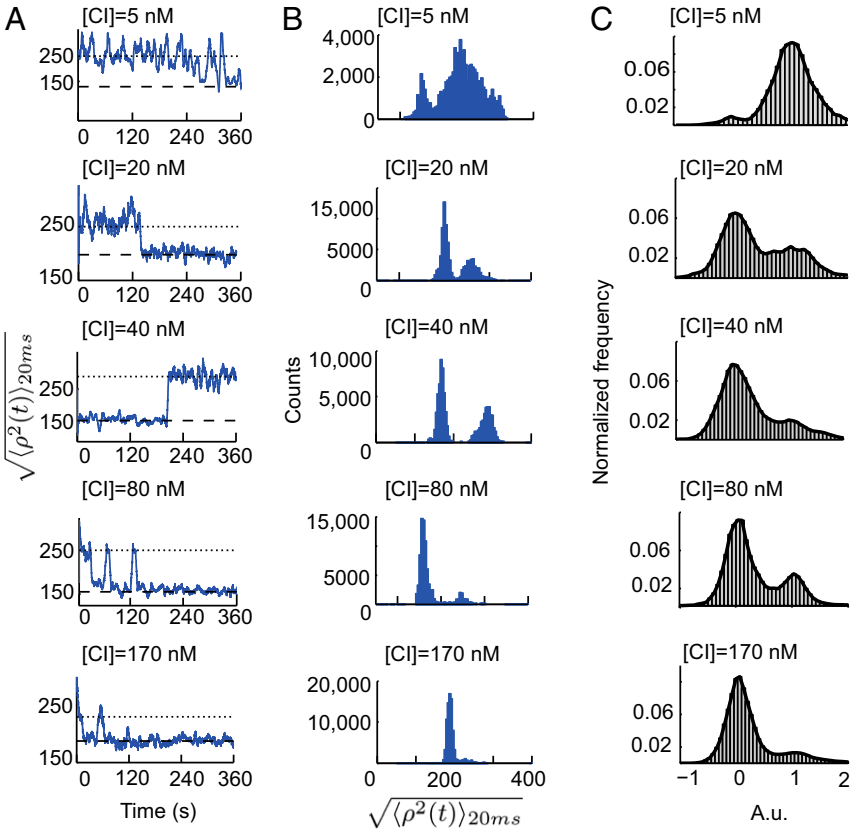

Fig. 3. Tethered particle motion time series signal and histograms of the looped and unlooped state for different CI concentrations using the pSB4357 plasmid. (*A*) Effective length of tether, $\sqrt{\langle \rho^2(t) \rangle_{20ms}}$, plotted as a function of time for beads tethered by a supercoiled plasmid. The plotted lines in the trajectory indicate the average excursions for unlooped (dotted line) and looped (dashed line). (*B*) Histograms of the time series shown in *A* (same abscissa for all concentrations). (*C*) Normalized collapsed histograms of looped and unlooped states, represented by the values 0 and 1, respectively, from all obtained datasets (same abscissa for all concentrations). The number of datasets for each concentration is $n = 4$ for 5 nM CI, $n = 7$ for 20 nM CI, $n = 5$ for 40 nM CI, $n = 6$ for 80 nM CI, and $n = 9$ for 170 nM CI, and significantly longer time series were used for the analysis than here shown. The looping probability increases as a function of CI concentration.

of the tether varied accordingly and the absolute value of $\sqrt{\langle \rho^2(t) \rangle_{20ms}}$ did not carry information on whether the plasmid was looped or not. However, a typical time series would show two distinct states (assigned to the looped and the unlooped form) and transitions between these two states. Therefore, we used the characteristic two-states shown in the time series to identify the looped and unlooped states. If no transitions were observed, the time series was not analyzed with respect to CI-mediated looping (which might give rise to an underestimation of looping at [CI] = 170 nM, where the plasmid could remain constantly looped during the entire observation period). To collapse all time series into a single histogram, we performed a linear transformation of the position histograms by designating a value of 0 to the peak of the distribution originating from the looped state (on histograms as shown in Fig. 3*B*) and a value of 1 to the peak of the unlooped state. The result of the data collapse for each CI concentration is shown in Fig. 3*C*. The data were fitted by two Gaussian distributions, one for the looped and one for the unlooped state. The looping probabilities were calculated as the ratio between the area under the Gaussian curve representing the looped state and the total area of the histogram. The uncertainties of the measured loop probabilities were determined by error propagation of the 95% confidence interval of the Gaussian fitting parameters as detailed in *SI Text*.

From Fig. 3*C* it is seen that the probability of looping increased as the concentration of CI increased. The observation that loop formation was negligible at low CI concentrations was expected because it was unlikely that the two operators, OL and OR, would be occupied simultaneously by CI. As CI concentration increased, octamer/octamer+tetramer complexes stabilized the loop configuration until saturation of the operator sites occurred and there was only little effect of increasing the concentration further (from 80 nM to 170 nM CI). The experiment depicted in Fig. 3*C* found the equilibrium between looped and unlooped states shifts toward more plasmids being in the looped state as CI concentration was increased.

The result of quantifying looping probabilities as function of CI concentration is shown in Fig. 4*A*, where the solid red circles denote data from CI-mediated looping of supercoiled plasmids. For comparison, we also plotted data on looping probability of linear DNA (solid blue squares) reported by Zurla et al. (14). Clearly, supercoiled DNA responded differently to CI concentration than linear DNA responded. In particular, the CI concentration interval where both the looped and unlooped states were significantly populated became narrower with supercoiled DNA than with linear DNA. A sharp response to changing CI concentration is expected for a regulatory network displaying a binary response. This is in contrast to metabolic pathways whose expression scales with nutrient availability as in the case of lactose utilization (31).

To investigate whether the difference in CI-mediated looping was due to the circular nature of the supercoiled plasmid, we examined looping in the relaxed form, pSB4357-R. To this end we chose the concentrations of CI that lead to the greatest difference in looping probability between linear and supercoiled DNA, 40 nM and 80 nM CI, and the results of looping probability are shown as open black triangles in Fig. 4*A*. The looping probability of relaxed pSB4357-R appeared similar to that reported for linear DNA (14). This observation suggests the difference between looping probability of supercoiled DNA and linear DNA is due to supercoiling rather than the circular nature of the supercoiled plasmid.

Thermodynamic Model. To further investigate the stability of the λ switch in a supercoiled system, we analyzed our data in the light of a thermodynamic model first put forward in ref. 20 and later modified to account for DNA looping (21, 22). The model relates the probability of each operator configuration to a given measure of the free CI monomer concentration. Details of the model can

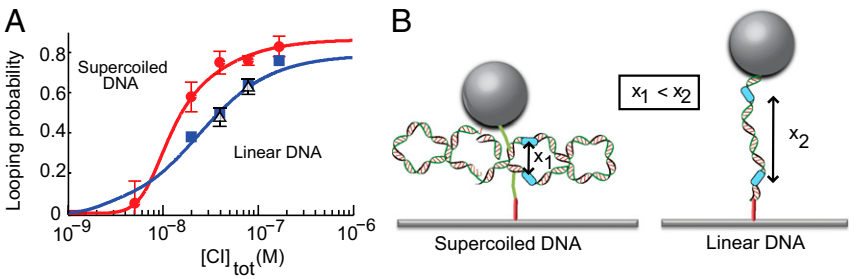

Fig. 4. Looping probability as a function of CI concentration for supercoiled DNA and linear relaxed DNA. (*A*) Data obtained from CI-mediated looping of supercoiled DNA plasmids are shown as solid red circles. Data from CI-mediated looping of linear DNA (solid blue squares) were published by Zurla et al. (14). The hollow black triangles denote data from the relaxed plasmid pSB4357-R, which coincide with the results from linear DNA. Lines show fits of the modified thermodynamic model to data from the supercoiled assay (red) and of the original model to the linear assay (14) (blue), respectively. Error bars represent SD. (*B*) Illustration of difference between supercoiled and linear assay, on average the effective distance between the two operator sites, OL and OR (marked by blue rectangles), is significantly shorter in the supercoiled configuration (x_1) than in the linear configuration (x_2). The relaxed pSB4357-R is identical to the structure shown on the left but without supercoils.

be found in ref. 14 and in *SI Text*; the blue line in Fig. 4*A* shows a fit of the model to looping data of linear DNA using the parameters found in ref. 14. Protein-mediated looping introduces two cooperative free energy terms: ΔG_{oct} and ΔG_{tetr}. ΔG_{oct} reflects the net free energy change due to octamerization of CI bound across OL1–OR1–OL2–OR2, together with the cost of formation of a DNA loop: $\Delta G_{oct} = \Delta G_{oct}^{(P)} - RT \ln(\Delta S_{loop})$. Here $\Delta G_{oct}^{(P)}$ is the cooperative free energy associated with octamer interactions and $-RT \ln(\Delta S_{loop})$ the entropic part of the free energy associated with DNA looping. ΔG_{tetr} reflects the cooperative free energy due to tetramerization of CI bound across OL3–OR3 and is only added if a loop is present and CI binds to the two remaining operators, thus forming an octamer–tetramer complex. As the previous model (14) (blue line in Fig. 4*A*) was optimized to fit a linear DNA, a modification was needed to adapt the model to our data collected with supercoiled DNA. In the supercoiled state, fewer conformations are available than for the linear state and all states are more rapidly explored. Hence, OR and OL are more frequently in proximity (as illustrated in Fig. 4*B*) and supercoiling enhances loop probability by lowering entropy costs. Therefore, ΔG_{oct} was decreased from 1.7 kcal/mol to 0 kcal/mol and ΔG_{tetr} was set to –1.0 kcal/mol instead of –2.4 kcal/mol. $\Delta G_{oct} = 0$ kcal/mol is in good agreement with free energies reported in vivo (~ -0.5 kcal/mol) (21, 22). The sum of the free energies $\Delta G_{complex} = \Delta G_{oct} + \Delta G_{tetr} = -1.0$ kcal/mol indicates that looping on supercoiled DNA is energetically more favorable than on linear DNA ($\Delta G_{complex} = -0.3$ kcal/mol); a comparison of the values of ΔG_{oct} and ΔG_{tetr} from the literature is given in Table 1. A second modification of the thermodynamic parameters entering the model was that we decreased the binding energies for all operator sites while keeping the cooperative parameters constant; the reasoning behind this is that gene regulation is commonly found to be sensitive to supercoiling (32), as it can change the local structure of DNA and influence protein DNA binding. In practice we weakened all binding energies between CI dimers and operator sites by 1.5 kcal/mol.

A fit of the model adopted to include supercoiling is shown as a red line in Fig. 4*A*. Another way of quantifying the cooperativity is to fit the Hill function to the data. This yields a Hill coefficient of 2.5 for the supercoiled data compared with 1.2 for the linear data (14). Cooperativity is a consequence of the binding of multiple proteins simultaneously and is essential for switch efficiency, as it steepens the transition.

Table 1. Comparison of free energies

Reference	ΔG_{oct}, kcal/mol	ΔG_{tetr}, kcal/mol
Current study	0	–1.0
Zurla et al. (14)	1.7	–2.4
Dodd et al. (22)	–0.5	–3

This pronounced bistable nature of the supercoiled system is in accordance with the nature of the λ phage: Once the λ phage has committed to enter either the lysogenic or the lytic state, the commitment is complete. Not only is the lysogenic state extremely stable in the supercoiled system, but when the host is exposed to inducing factors, switching to the lytic state can be efficiently done upon only a small change in CI concentration. In conclusion, our data show that natively supercoiled DNA provides an efficient and stable λ switch.

Discussion

We developed a PNA-based assay that allowed us to tether supercoiled plasmids between cover slides and beads. We investigated the internal dynamics of individual DNA tethers, both supercoiled plasmids, relaxed plasmids, and linear tethers, as well as protein-mediated DNA looping in a supercoiled system.

The RMSDs of supercoiled, relaxed, and linear DNA were compared, and it was found that the RMSD of the entangled supercoiled plasmid was significantly smaller than those of the relaxed plasmid and linear tether, which were comparable. Further, we found that the supercoiled plasmid exhibited a much faster relaxation time than the relaxed plasmid and the linear tether, which is analogous to enhanced site juxtaposition in the supercoiled state. These findings support previously published molecular dynamics simulations (19) and in vitro transcription assays (18).

The thermodynamic parameters of DNA looping have previously been studied in vivo (21, 22) and by single molecule experiments using linear DNA (14). In the latter study using linear DNA, the results showed that DNA looping involving six operators and six CI dimers was relative stable, whereas looping involving only four dimers (without OR3 and OL3 being occupied) was less stable. It appears that supercoiling of DNA enhances loop stability in comparison with looping of a linear DNA tether. The experimental result is supported by the fact that the thermodynamic model provided an excellent fit to the in vitro supercoiled DNA experimental data, yielding parameters consistent with in vivo observations (21, 22). A more recent in vitro study using supercoiled templates in a transcription assay has confirmed the enhancement of pRM activation by the octamer-mediated loop and the cooperative role of OL3 and OR3 in pRM repression (12). These findings indicate supercoiling increases the loop stability as directly observed here.

In summary, we have developed a single molecule assay using natively supercoiled DNA. We investigated the looping probabilities as a function of CI concentration and found a sharper transition between looped and unlooped states than observed with linear DNA (14). This sharper transition is expected for the regulatory network deciding between lytic and lysogenic states. By fitting a thermodynamic model to our data, we obtained values for the free energies associated with loop formation that were consistent with values reported for in vivo natively supercoiled DNA. Our work provides crucial insight into how supercoiling changes the dynamics of the lambda switch, the first epigenetic switch to

be deciphered and the switch that has become a paradigm for transcriptional regulation.

Materials and Methods

DNA. All plasmids were prepared as monomers in the recombination-deficient strain, SS74 (5). pSB4293, pSB4300, and pSB4312 all bear the BamHI to EcoRI fragment of λ (nucleotides 34,500–39,168) containing the immunity region and the early phage terminators replacing the BamHI–EcoRI fragment of pBluescriptKS(–) (Stratagene). The target for PNA1021, 5′-AAGAAGAAAA-3′, was placed adjacent to λ nucleotide 34,500 in pSB4293 and pSB4312. The target of PNA3593, 5′-AGAGAAAGAA-3′, was placed adjacent to λ nucleotide 39,168 in pSB4300 and pSB43412. pSB4357 is similar to pSB4312 but bears λ DNA from 35,517–38,126, placing OL and OR closer to the PNA targets. The 2.6 kbp linear DNA was prepared by PCR amplification of λ DNA representing nucleotides 35,501–38,140, with primers bearing 5′-biotin and 5′-digoxygenin. Oligonucleotides and methods are described in *SI Text*.

PNA. The bis-PNAs PNA1021 [Biotin-$(eg1)_3$-TTJ TTJ TTTTLys-aha-Lys-aha-Lys-TTTT CTT CTT-Lys-NH_2] (23) and PNA3593 [Dig-$(eg1)_3$-$(DMLys)_3$-TJT JTT TJT T-$(eg1)_3$-TTC TTT CTC T-Gly-NH_2 (DMLys = ε-N,*N*-dimethyl lysine; aha = 6-aminohaxanoic acid, eg1 = 8-amino-3,6-oxaoctanoic acid)] were synthesized using solid phase Boc chemistry according to published procedures (23, 33, 34). Digoxigenin was conjugated to the bis-PNA in solution using Digoxigenin NHS-ester. PNAs were purified by HPLC and characterized by MALDI-TOF mass spectrometry.

Chloroquine Gel Analysis of Supercoiling. Samples were electrophoresed through 1% agarose in Tris-acetate EDTA buffer supplemented with 3 μg/mL chloroquine-diphosphate as described by ref. 35 and stained with ethidium bromide (Fig. 2*C* and Fig. S4).

Preparation of DNA–PNA-Bead Complex and Flow Chambers. Triplex invasion of PNA and DNA was executed by incubating a 20-fold excess of PNA, 17 nM DNA with 0.33 μM PNA1021 (biotin labeled) and 0.33 μM PNA3593 (digoxigenin labeled), in (PEN buffer) 10 mM sodium Pipes pH 6.5, 0.1 mM EDTA, and 10 mM NaCl for 14–15 h at 37 °C in an air incubator (23). After incubation the DNA–PNA complex was diluted 25-fold in PEN buffer and stored at 5 °C until use. Before use, the DNA–PNA complex was further diluted (25-fold) in λ buffer (10 mM Tris·HCl pH 7.4, 200 mM KCl, 0.1 mM EDTA, 0.2 mM DTT). To remove nonspecifically formed triplex invasion complexes, the samples were incubated at 65 °C for 10 min in a water bath (23). A rectangular perfusion chamber (~15 μL) was created by joining two cover slides by two melted strips of parafilm. We perfused 20 μL of 20 μg/mL antidigoxigenin dissolved in PBS buffer into the chamber and incubated it for 30 min at room temperature. Then, the chamber was incubated with 20 μL of 2 mg/mL α-casein in λ buffer for 30 min at room temperature to passivate the surface. Hereafter, it was incubated with 20 μL of the prepared DNA–PNA complex for 60 min at room temperature, allowing the digoxigenin-labeled PNA to bind to the antidigoxigenin-coated surface. Finally, the chamber was incubated with 20 μL containing an excess of streptavidin-coated beads in 2 mg/mL α-casein dissolved in PBS for 30 min at room temperature. This allowed the biotin-labeled PNA end to bind to a streptavidin-coated bead. Between each exchange the chamber was washed with 90 μL of λ buffer. In looping experiments, the chamber was filled with 20 of μL CI diluted to the required concentration before sealing the chamber. Experiments were initiated after 10 min of incubation.

CI Protein. The λ repressor protein (CI) used in this work was expressed, purified, and generously provided by Dale Lewis and Sankar Adhya (Laboratory of Molecular Biology, Center for Cancer Research, National Cancer Institute, National Institutes of Health, Bethesda, MD). CI was stored in λ buffer at –20 °C in small aliquots and only thawed and diluted immediately before use.

Single Particle Tracking Experiments and Analysis Method. Images of the tethered beads were recorded via a progressive scan camera mounted on an inverted microscope equipped with a 100× oil immersion objective. Movement of the tethered particle was examined by Principal Component Analysis (PCA) to calculate the RMSD of a bead and its excursion symmetry (*s*) as detailed in *SI Text*.

ACKNOWLEDGMENTS. The CI protein was generously provided by Dale Lewis and Sankar Adhya (Laboratory of Molecular Biology, Center for Cancer Research, National Cancer Institute, National Institutes of Health, Bethesda, MD). The MatLab-based thermodynamic model was generously provided by Carlo Manzo (Single Molecule Biophotonics, The Institute of Photonic Sciences, Barcelona, Spain) and Laura Finzi (Department of Physics, Computational and Life Science Core Faculty, Emory University, Atlanta, GA). We also thank Thomas Bentin for advice on handling PNAs. This research was funded by the Excellence Program at the University of Copenhagen.

1. Ptashne M (2004) *A Genetic Switch: Phage Lambda Revisited* (Cold Spring Harbor Lab Press, Cold Spring Harbor, NY), 3rd Ed.
2. Ptashne M (2011) Principles of a switch. *Nat Chem Biol* 7(8):484–487.
3. Thompson JN (2012) Evolution. The role of coevolution. *Science* 335(6067):410–411.
4. Brooks K, Clark AJ (1967) Behavior of λ bacteriophage in a recombination deficienct strain of Escherichia coli. *J Virol* 1(2):283–293.
5. Baek K, Svenningsen S, Eisen H, Sneppen K, Brown S (2003) Single-cell analysis of lambda immunity regulation. *J Mol Biol* 334(3):363–372.
6. Little JW, Michalowski CB (2010) Stability and instability in the lysogenic state of phage lambda. *J Bacteriol* 192(22):6064–6076.
7. Wang H, Finzi L, Lewis DE, Dunlap D (2009) AFM studies of lambda repressor oligomers securing DNA loops. *Curr Pharm Biotechnol* 10(5):494–501.
8. Révet B, von Wilcken-Bergmann B, Bessert H, Barker A, Müller-Hill B (1999) Four dimers of lambda repressor bound to two suitably spaced pairs of lambda operators form octamers and DNA loops over large distances. *Curr Biol* 9(3):151–154.
9. Kim B, Little JW (1993) LexA and lambda CI repressors as enzymes: Specific cleavage in an intermolecular reaction. *Cell* 73(6):1165–1173.
10. Espejo RT, Canelo ES, Sinsheimer RL (1969) DNA of bacteriophage PM2: A closed circular double-stranded molecule. *Proc Natl Acad Sci USA* 63(4):1164–1168.
11. Manzo C, Zurla C, Dunlap DD, Finzi L (2012) The effect of nonspecific binding of lambda repressor on DNA looping dynamics. *Biophys J* 103(8):1753–1761.
12. Lewis D, Le P, Zurla C, Finzi L, Adhya S (2011) Multilevel autoregulation of λ repressor protein CI by DNA looping in vitro. *Proc Natl Acad Sci USA* 108(36):14807–14812.
13. Zurla C, et al. (2006) Novel tethered particle motion analysis of CI protein-mediated DNA looping in the regulation of bacteriophage lambda. *J Phys Condens Matter* 18(14):S225–S234.
14. Zurla C, et al. (2009) Direct demonstration and quantification of long-range DNA looping by the lambda bacteriophage repressor. *Nucleic Acids Res* 37(9):2789–2795.
15. Lia G, et al. (2008) The antiparallel loops in gal DNA. *Nucleic Acids Res* 36(12):4204–4210.
16. Normanno D, Vanzi F, Pavone FS (2008) Single-molecule manipulation reveals supercoiling-dependent modulation of lac repressor-mediated DNA looping. *Nucleic Acids Res* 36(8):2505–2513.
17. Lia G, et al. (2003) Supercoiling and denaturation in Gal repressor/heat unstable nucleoid protein (HU)-mediated DNA looping. *Proc Natl Acad Sci USA* 100(20):11373–11377.
18. Polikanov YS, et al. (2007) Probability of the site juxtaposition determines the rate of protein-mediated DNA looping. *Biophys J* 93(8):2726–2731.
19. Jian H, Schlick T, Vologodskii A (1998) Internal motion of supercoiled DNA: Brownian dynamics simulations of site juxtaposition. *J Mol Biol* 284(2):287–296.
20. Ackers GK, Johnson AD, Shea MA (1982) Quantitative model for gene regulation by lambda phage repressor. *Proc Natl Acad Sci USA* 79(4):1129–1133.
21. Anderson LM, Yang H (2008) DNA looping can enhance lysogenic CI transcription in phage lambda. *Proc Natl Acad Sci USA* 105(15):5827–5832.
22. Dodd IB, et al. (2004) Cooperativity in long-range gene regulation by the lambda CI repressor. *Genes Dev* 18(3):344–354.
23. Bentin T, Nielsen PE (2002) In vitro transcription of a torsionally constrained template. *Nucleic Acids Res* 30(3):803–809.
24. Nielsen PE, Egholm M, Berg RH, Buchardt O (1991) Sequence-selective recognition of DNA by strand displacement with a thymine-substituted polyamide. *Science* 254(5037):1497–1500.
25. Tolić-Nørrelykke SF, Rasmussen MB, Pavone FS, Berg-Sørensen K, Oddershede LB (2006) Stepwise bending of DNA by a single TATA-box binding protein. *Biophys J* 90(10):3694–3703.
26. Bentin T, Nielsen PE (1996) Enhanced peptide nucleic acid binding to supercoiled DNA: Possible implications for DNA "breathing" dynamics. *Biochemistry* 35(27):8863–8869.
27. Blumberg S, Gajraj A, Pennington MW, Meiners JC (2005) Three-dimensional characterization of tethered microspheres by total internal reflection fluorescence microscopy. *Biophys J* 89(2):1272–1281.
28. Liu Y, Bondarenko V, Ninfa A, Studitsky VM (2001) DNA supercoiling allows enhancer action over a large distance. *Proc Natl Acad Sci USA* 98(26):14883–14888.
29. Reichardt L, Kaiser AD (1971) Control of lambda repressor synthesis. *Proc Natl Acad Sci USA* 68(9):2185–2189.
30. Aurell E, Brown S, Johanson J, Sneppen K (2002) Stability puzzles in phage lambda. *Phys Rev E Stat Nonlin Soft Matter Phys* 65(5 Pt 1):051914.
31. Clark DJ, Marr AG (1964) Studies on the repression of beta-galactosidase in escherichia coli. *Biochim Biophys Acta* 92:85–94.
32. DiNardo S, Voelkel KA, Sternglanz R, Reynolds AE, Wright A (1982) Escherichia coli DNA topoisomerase I mutants have compensatory mutations in DNA gyrase genes. *Cell* 31(1):43–51.
33. Christensen L, et al. (1995) Solid-phase synthesis of peptide nucleic acids. *J Pept Sci* 1(3):175–183.
34. Egholm M, et al. (1995) Efficient pH-independent sequence-specific DNA binding by pseudoisocytosine-containing bis-PNA. *Nucleic Acids Res* 23(2):217–222.
35. Esposito F, Sinden RR (1987) Supercoiling in prokaryotic and eukaryotic DNA: Changes in response to topological perturbation of plasmids in E. coli and SV40 in vitro, in nuclei and in CV-1 cells. *Nucleic Acids Res* 15(13):5105–5124.